Modeling Hyperfine Coupling in Molecular Magnets

Alice Hu[1], Jia Chen[2], Xiaoguang Zhang[2]

[1]Department of Physics, University of Connecticut, Storrs

[2]Department of Physics, University of Florida

Abstract

Algorithms devised by Shor and Grover have demonstrated that a quantum computer factors numbers and searches databases much faster than a classical computer. Researchers have shown that molecular magnets are excellent candidates for quantum bits (qubits) [1], using either their nuclear or electron spins. Electron spins are advantageous due to their faster operational times; however, they decohere faster. Hyperfine coupling is the main cause of decoherence in magnetic molecules. This project tries to investigate the effect of hyperfine coupling on electron spin decoherence. Hyperfine coupling values were calculated using density functional theory and compared with experimental values. The Kubo-Anderson model was applied to link hyperfine coupling with the coherence time T_2. The theoretical T_2 was compared with experimental values. The simple theory of random frequency modulation is not adequate to explain decoherence time observed in a series of vanadyl complexes. Decoherence of electron spins in molecular complexes shows interesting physics that warrants further investigation.

Introduction

Quantum computing (QC) is of great interest to the scientific community due to its potential to solve quantum problems, which could lead to new breakthroughs in the fields of materials discovery, medicine, and machine learning [2]. A QC stores all the information of a wavefunction and uses quantum-mechanical principles, such as entanglement and superposition, to perform computations. Since it operates using the same quantum principles as atoms and molecules, QCs can calculate all of their quantum properties [2]. If a researcher can measure the bits before decoherence, they will obtain the direct quantum solution.

Unlike traditional computers composed of bits with a value of either 0 or 1, quantum computers have qubits that are superpositions of two quantum states (see Fig. 1). One way to represent these quantum states is by using either an electron or nuclear spin.

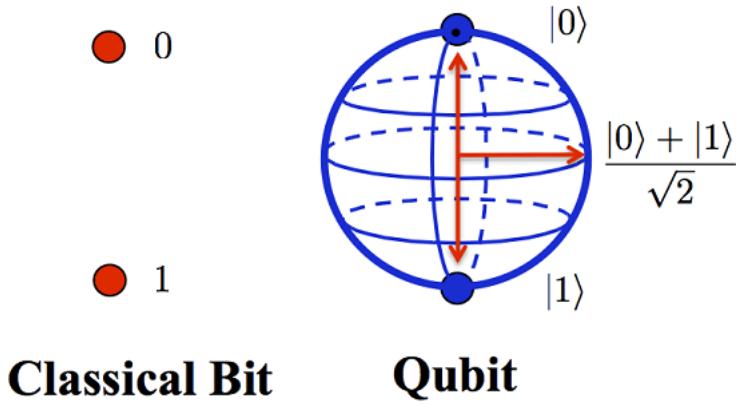

Fig. 1 A diagram illustrating the difference between classical and quantum computers [3].

Currently, nuclear spins are preferred to electron spins because nuclear spins are generally coherent for longer [4-5]. The method of controlling nuclear spins—Nuclear Magnetic Resonance (NMR)—requires a large magnetic field while electron spin-based QCs do not. To detect and control electron spins, Electron Paramagnetic Resonance (EPR) is used. Unfortunately, the theory of decoherence for EPR is not as developed as for NMR. This project

took the first step in addressing this gap by applying established theory from NMR to EPR and finding out what can be applied.

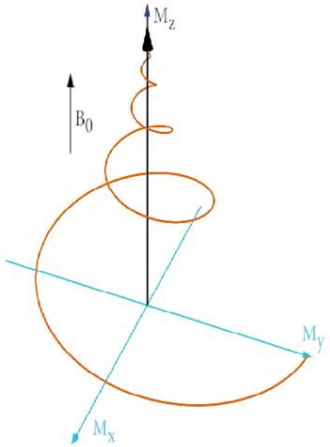

Fig. 2 The path that the magnetization vector $\vec{M}$ points in.

In NMR, there are two relaxation times commonly measured during experiments: T_1 and T_2. Fig. 2 shows the relaxation path of the magnetization vector. T_1 is associated with the longitudinal relaxation of magnetization, in the direction of external magnetic field B_0. T_2 is associated with the transverse relaxation of magnetization, perpendicular to external magnetic field B_0. T_2 is used to determine how long the system stays coherent. This project focuses on finding a relationship between hyperfine coupling (HC) and T_2. For a molecule to be used as a qubit, it needs a long relaxation time to hold and allow the quantum information to be measured.

One mechanism that can induce decoherence is the hyperfine coupling—interactions between electron and nuclear spins. Random magnetic fields from nuclear spins can cause the electron spins to decohere. In the HC there are two contributing interactions: spin-dipole (SD) and Fermi contact (FC). The spin-dipole interaction is analogous to the interactions between dipoles in classical electrodynamics. In this case it is when the magnetic moments of the electron and nuclear spins interact. Fermi contact is when the electron and nuclear wavefunctions overlap. This happens through s orbital contributions of unpaired electrons.

The HC has been shown to contribute to the decoherence in quantum dots [6]. To explain how HC contributes to decoherence in molecules, this project applied the Kubo-Anderson (random frequency-modulation) model—a general theory of relaxation [7-8]. This theory was applied by modeling nuclear spins as a perturbation. We used this to model the decoherence of electron spins in four vanadyl complexes, but the theoretical T_2 values were off from the experimental T_2 values. This is due to the diffusion barrier radius—when HC is so strong that the electron spin flip-flops do not occur on the timescale of decoherence—which needs to be accounted for. Once there is an accurate theory for decoherence, it may be possible to engineer molecules to maximize the coherence time.

Computational Details

One potential qubit candidate that has been identified is a type of vanadyl complex [9]. They all have the same charge and spin. Their electron spins were identified as potential qubits. This experiment focused on determining how the nuclear spin distances (from the hydrogen atoms to the vanadium atom) affected the electron spin decoherence.

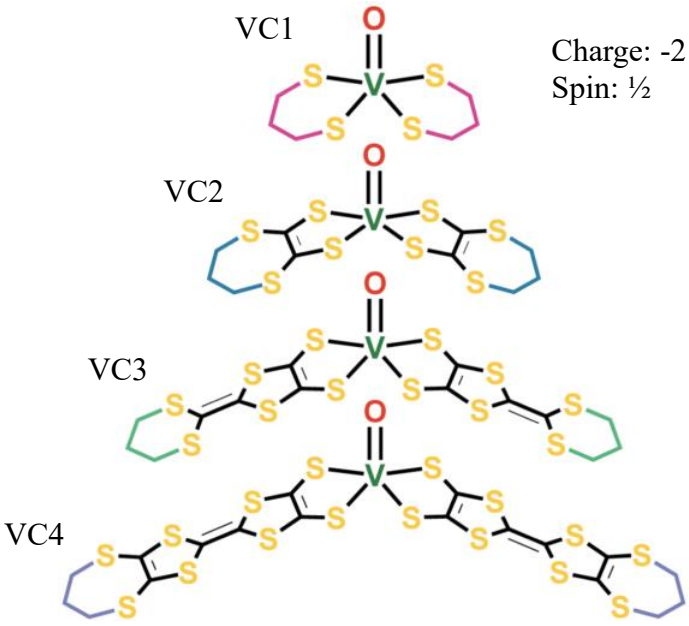

Fig. 3 Schematic of four vanadyl complexes in this study [9]. The electron spin is centered on the vanadium atom. Three nuclear spins that contribute to decoherence are on the end of each ligand attached to vanadium.

Theoretical values of the HC constants were calculated using two quantum chemistry methods: density functional theory (DFT) and Hartree Fock (HF). DFT is widely used because it balances speed and accuracy. In DFT the functional uses the electron density to determine the total energy of the system. Two functionals were used in this study: BP and B3LYP. BP is at the level of the generalized gradient approximation (GGA). By taking the density and the gradient of the electron density, one can model molecules where the density quickly changes. This is commonly used by materials scientists modelling metals. B3LYP is a hybrid functional, which means it combines DFT with HF. This is most often used by chemists modelling molecules.

DFT approximates the exchange and correlation of electrons. Exchange is the part of the electron-electron interaction that arises from the electrons being indistinguishable particles. Correlation is another part of the electron-electron interaction. HF exactly models the exchange, but it completely ignores the correlation between electrons. Combining the two gives a more accurate result than when they are used separately.

The wavefunction is represented approximately via basis sets in DFT. CP(PPP) [10] was used for vanadium and TZVP was used for all other atoms. Using a DFT package called ORCA [11], unrestricted DFT was performed. Unrestricted DFT means that the electrons are not forced to pair up. The grid accuracy was increased for vanadium, because it is the atom of most interest. The convergence was set to slow. Simulations were run in parallel using four cores.

Theory

I. Classical Equation of Motion for Spin

In NMR and EPR experiments, there is a static uniform external magnetic field pointing in the z-direction and experimentalists can control the magnetization by radio frequency or microwave pulse in the xy-plane and measure how it changes with time. To begin to interpret their measurements, a classical description of spin motion in a magnetic field can be used.

A magnetic moment $\vec{\mu}$ in a static magnetic field $\vec{B}$ experiences a torque $\vec{\mu} \times \vec{B}$. Torque is the rate of change of the angular momentum, so the equation of motion for spin angular momentum is:

$$\vec{\mu} \times \vec{B} = \hbar \dot{\vec{I}}. \tag{1}$$

The magnetic moment is proportional to angular momentum:

$$\overrightarrow{\mu} = \gamma \hbar \vec{I}, \tag{2}$$

where γ is gyromagnetic ratio for nuclear or electron spins. Eqs. (1) and (2) imply that the equation of motion for the magnetic moment becomes:

$$\dot{\vec{\mu}} = \gamma \, \vec{\mu} \times \vec{B}. \tag{3}$$

If there is an ensemble of non-interacting spins, then the total magnetization is the sum of magnetic moments:

$$\overrightarrow{M} = \frac{1}{V} \sum_i \overrightarrow{\mu}_i. \tag{4}$$

It obeys the same equation of motion as an individual magnetic moment:

$$\dot{\vec{M}} = \gamma \, \vec{M} \times \vec{B}. \tag{5}$$

This equation can be solved once the direction of $\vec{B}$ is specified. If it is in the z-direction:

$$\vec{B} = B_0 \hat{z}, \tag{6}$$

the three components of the equation of motion are:

$$\dot{M}_x = \gamma B_0 M_y, \tag{7}$$

$$\dot{M}_y = -\gamma B_0 M_x, \tag{8}$$

$$M_z = 0. \tag{9}$$

Assuming the initial condition $M_y(0) = 0$, the solution becomes:

$$M_x(t) = M_x(0)\cos(\gamma B_0 t), \tag{10}$$

$$M_y(t) = -M_x(0)\sin(\gamma B_0 t), \tag{11}$$

$$M_z(t) = M_z(0). \tag{12}$$

These equations model rotation in the xy-plane with a constant z-component. This motion is called Larmor precession. The precession frequency γB_0 in the xy-plane is the Larmor frequency.

The set of initial conditions $M_y(0) = 0, M_z(0) = 0$, and $M_x(0) = M(0)$ can be achieved using radio-frequency (RF) pulses. After the RF pulse, the magnetization relaxes and eventually goes to its equilibrium value, which is zero in the xy-plane and M_{eq} in the z-direction.

Using a phenomenological approach, the relaxation terms are added to the precession equations:

$$\dot{M}_x = \gamma|\vec{M} \times \vec{B}\big|_x - \frac{M_x}{T_2}, \tag{13}$$

$$\dot{M}_y = \gamma|\vec{M} \times \vec{B}\big|_y - \frac{M_y}{T_2}, \tag{14}$$

$$\dot{M}_z = \gamma|\vec{M} \times \vec{B}\big|_z - \frac{M_z - M_{eq}}{T_1}. \tag{15}$$

These three equations are called the Bloch equations [12], which can be used to interpret NMR and EPR data. T_1 and T_2 are usually referred to as the longitudinal and transverse relaxation times, or spin-lattice and spin-spin relaxation time for historical reasons. Given the initial condition mentioned before and a constant magnetic field B_0 in z-direction, the solution of Bloch equations is:

$$M_x(t) = M(0)\cos(\omega_0 t)\exp\left(-\frac{t}{T_2}\right), \quad (16)$$

$$M_y(t) = -M(0)\sin(\omega_0 t)\exp\left(-\frac{t}{T_2}\right), \quad (17)$$

$$M_z(t) = M_{eq}\left(1 - \exp(-\frac{t}{T_1})\right). \quad (18)$$

In the xy-plane, besides precession, we have an exponential decay function to modulate the oscillations. This is the relaxation function, which will be the focus of this work:

$$\phi(t) = \exp(-\frac{t}{T}). \quad (19)$$

Doing a Fourier transform results in the resonance absorption line shape:

$$I(\omega - \omega_0) = \frac{1}{2\pi}\int_{-\infty}^{\infty} e^{-i(\omega-\omega_0)t}\phi(t)dt. \quad (20)$$

II. Stochastic Theory for Transverse Relaxation

When solids were first measured using NMR, experimentalists noticed that the transverse relaxation was caused by the inhomogeneity of the magnetic field (local field effect) [13]. However, when we focus on the spins of individual molecules, each one has its own local magnetic field, which changes due to their environment and motion. Since the magnetic field is proportional to the Larmor frequency, each spin precesses at a slightly different frequency. These small frequency differences cause decoherence of precession and transverse relaxation.

One way to treat the local field effect is to model the local field as a stochastic variable. This general theory of relaxation is called the Kubo-Anderson model (Random frequency-modulation model) [7-8]. The slow modulation limit of this model is used here to calculate the transverse relaxation time for the vanadyl complex.

A complex magnetic moment in the xy-plane can be defined as:

$$\mu = \mu_x + i\mu_y. \quad (21)$$

So the equation of motion for complex magnetic moment is:

$$\dot{\mu_j}(t) = -i\gamma\left(B_0 + b_j\right)\mu_j(t). \tag{22}$$

Simplifying the magnetic field B_0 and gyromagnetic ratio b_j into a frequency, $\omega = -\gamma B$, we get the first part of the random frequency-modulation model:

$$\dot{\mu_j}(t) = i\omega(t)\mu, \tag{23}$$

where $\omega(t)$ is the frequency with random modulation.

The time average is defined as:

$$\omega_0 = \lim_{T\to\infty} \frac{1}{T}\int_0^T \omega(t)dt, \tag{24}$$

and ω_0 can be written as:

$$\omega(t) = \omega_0 + \omega_1(t). \tag{25}$$

$\omega(t)$ represents a random process that is time-independent and ergodic. The solution of Eq. 23 is:

$$\mu(t) = \mu_0 \exp\{i\int_0^t \omega(t')dt'\} \tag{26}$$

$$= \mu_0 \exp\{i\omega_0 t + i\int_0^t \omega_1(t')dt'\}. \tag{27}$$

Since $\omega(t)$ is a random process, $\mu(t)$ is also a random process. The ensemble average of $\mu(t)$ is:

$$\langle\mu(t)\rangle = \mu_0 e^{i\omega_0 t}\langle\exp\{i\int_0^t \omega_1(t')dt'\}\rangle. \tag{28}$$

Comparing Eq. 28 with Eq. 16, the relaxation function as defined by Eq. 20 is:

$$\phi(t) = \langle\exp\{i\int_0^t \omega_1(t')dt'\}\rangle. \tag{29}$$

Since $\omega_1(t)$ is a stochastic process, it has a probability distribution $\mathrm{P}(\omega')$. This gives us the probability density for finding the frequency at ω'. Usually a stochastic process is characterized by two parameters. The first one is amplitude of modulation:

$$\Delta^2 = \int \omega_1^2 \mathrm{P}(\omega_1)d\omega_1 = \langle\omega_1^2\rangle, \tag{30}$$

The second one is correlation time of modulation, defined using auto-correlation function:

$$\psi(\tau) = \frac{1}{\Delta^2}\langle\omega_1(t)\omega_1(t+\tau)\rangle. \quad (31)$$

The correlation time τ_c is:

$$\tau_c = \int_0^\infty \psi(t)dt. \quad (32)$$

In order to calculate the relaxation function, a moment (cumulant) expansion of Eq. 29 is used:

$$\begin{aligned}\phi(t) &= \langle\exp\left\{i\int_0^t \omega_1(t')dt'\right\}\rangle \\ &= \exp\left[i\int_0^t \omega_1(t')dt' - \frac{1}{2}\int_0^t dt_1\int_0^t dt_2\langle\omega_1(t_1)\omega_2(t_2)\rangle + \cdots\right].\end{aligned} \quad (33)$$

If the stochastic process $\omega_1(t)$ is a Gaussian process, this expansion to the second order is accurate to the fourth order. The first and third orders give zero and the second order is calculated as:

$$\begin{aligned}\phi(t) &= \exp[-\frac{1}{2}\int_0^t dt_1\int_0^t dt_2\langle\omega_1(t_1)\omega_2(t_2)\rangle] \\ &= \exp\left[-\frac{\Delta^2}{2}\int_0^t dt_1\int_0^t dt_2\psi(t_1-t_2)\right].\end{aligned} \quad (34)$$

By replacing variables, we arrive at the result:

$$\phi(t) = \exp[-\Delta^2\int_0^t d\tau(t-\tau)\psi(\tau)]. \quad (35)$$

Since the auto-correlation function is still unknown, approximations need to be made to actually do the calculation. The motion of particles in a solid can be modeled as harmonic oscillators. This means that correlation time τ_c is usually very long and $\Delta\cdot\tau_c \gg 1$. Kubo calls this the slow modulation case.

In the slow modulation case, we can approximate the auto-correlation function by $\psi(0) \approx \psi(t) = 1$. The integral in Eq. 35 then gives:

$$\phi(t) \approx \exp\left(-\frac{1}{2}\Delta^2 t^2\right). \quad (36)$$

Combining Eq. 19 and Eq. 36, in the slow modulation case transverse relaxation time T_2 is not precisely defined because Eq. 36 is not exactly an exponential decay function. T_2 is the time it takes for the relaxation function to drop to $\frac{1}{e}$ of its original value. Using that knowledge, T_2 can be estimated by the amplitude of modulation of the local field:

$$\frac{1}{T_2} \approx \sqrt{\frac{\Delta^2}{2}}. \tag{37}$$

The part of the Hamiltonian that results from the spin-dipole interaction is:

$$\mathrm{H} = \vec{I} \cdot \overleftrightarrow{A} \cdot \vec{S}. \tag{38}$$

Setting $\vec{I} \cdot \overleftrightarrow{A}$ equal to $\vec{B}$, $\vec{B}$ can be written in matrix form as:

$$\vec{B} = \begin{pmatrix} B_x \\ B_y \\ B_z \end{pmatrix}. \tag{39}$$

Writing it out in matrix form, the magnetic field is:

$$\vec{B} = \vec{I} \cdot \overleftrightarrow{A} = \begin{pmatrix} I\sin\theta\cos\psi \\ I\sin\theta\sin\psi \\ I\cos\theta \end{pmatrix} \begin{pmatrix} A_x & 0 & 0 \\ 0 & A_y & 0 \\ 0 & 0 & A_z \end{pmatrix}$$

$$= \begin{pmatrix} A_x I\sin\theta\cos\psi \\ A_y I\sin\theta\sin\psi \\ A_z I\cos\theta \end{pmatrix}. \tag{40}$$

Using Eq. 30, ω_1^2 is $\left(\vec{I} \cdot \overleftrightarrow{A}\right)^2 = \langle B^2 \rangle$ and $\mathrm{P}(\omega_1)$ is $\frac{1}{4\pi}$, which is from the surface area of a sphere. Eq. 30 becomes:

$$\Delta^2 = \int \left(\vec{I} \cdot \overleftrightarrow{A}\right)^2 \frac{1}{4\pi} d\omega_1. \tag{41}$$

The expectation values for $\langle B^2 \rangle$ are then:

$$\langle B_x^2 \rangle = \frac{4}{3}\pi A_x^2 I^2, \tag{42}$$

$$\langle B_y^2 \rangle = \frac{4}{3}\pi A_y^2 I^2, \tag{43}$$

$$\langle B_z^2 \rangle = \frac{2}{3} A_z^2 I^2. \quad (44)$$

Results

I. Electronic Structure

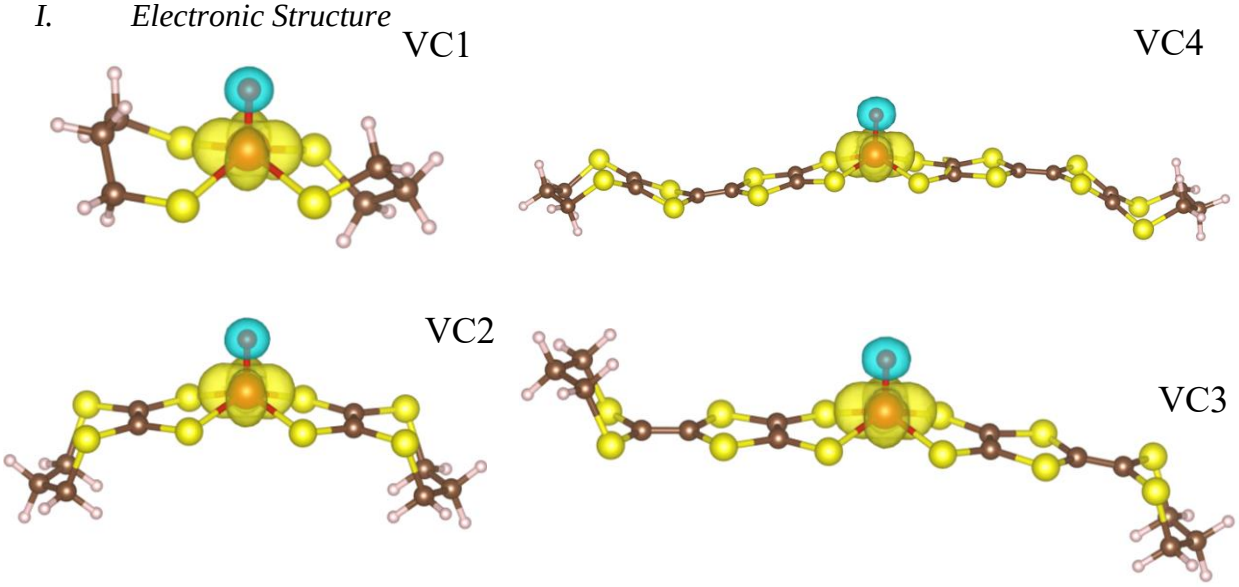

Fig. 4 Plot of net spin densities of vanadyl complexes. Yellow show the isosurface of majority spins; blue shows the isosurface of minority spins. The d orbitals are in the shape of yellow rounded four-leaf clovers and the s orbitals are the blue spheres.

As shown in Fig. 4, the spin densities behave like s and d orbitals localized around the oxygen and vanadium atoms. It is important because we will use this localized property to help the analysis of SD part of the HC. The net spin densities stay the same even as the size of the molecules grows.

Looking at Fig. 5 below, the HOMO-LUMO gap becomes smaller as the branch width (length of the longest V-H bond) grows. Since localized states are not dependent on size, this means that the vanadium states are not the highest occupied molecular orbitals (HOMO) or the lowest unoccupied molecular orbitals (LUMO). If these systems were electron or hole-doped, it would be expected that the local vanadium spin would be only slightly affected. This means that the analysis below would still be valid even if the electronic configuration is changed by doping.

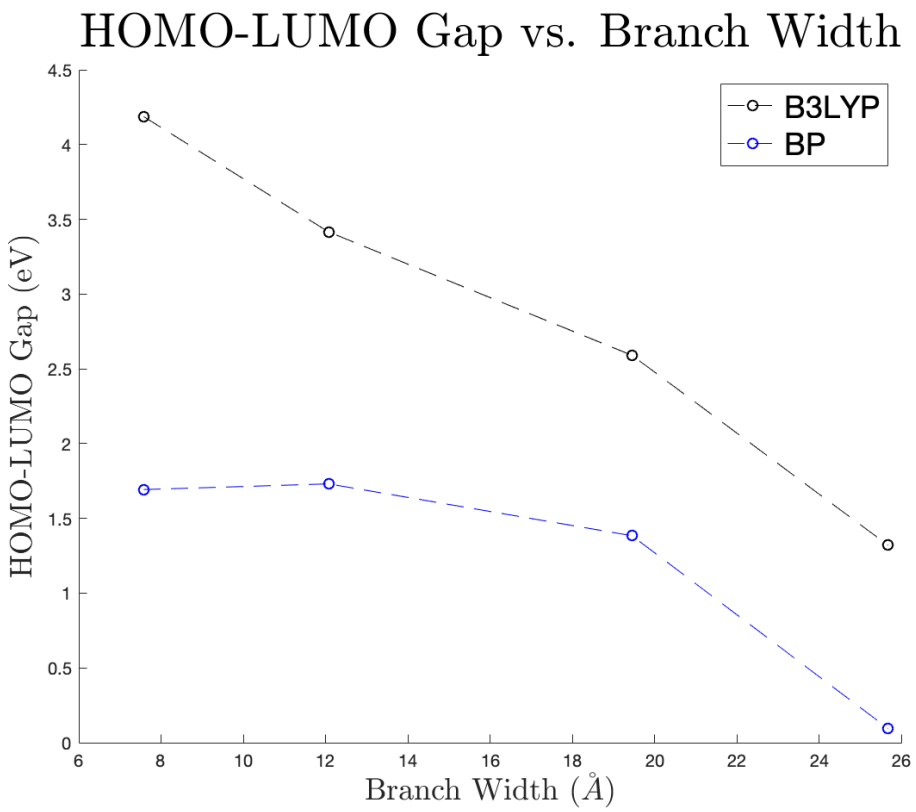

Fig. 5 Graph of the HOMO-LUMO Gap vs. Branch Width of VC. The branch width is the longest V-H bond in each VC. For both functionals it appears that the HOMO-LUMO gap decreases as branch width gets longer.

II. Hyperfine Couplings

Table 1. HC values for the vanadiums in the four VCs. SD and FC tabulated as well and two functionals BP & B3LYP are compared. The directions x, y, and z represent the two dipoles (electron and nuclear spins) both pointing in the x, y, and z directions respectively.

		Total		SD		FC	
		BP	B3LYP	BP	B3LYP	BP	B3LYP
VC1	x	-58.098	-76.337	93.8575	103.2613	-145.7124	-171.8776
	y	-70.2997	-87.624	82.1878	92.5145	-145.7124	-171.8776
	z	-336.3	-386.7	-176.045	-195.776	-145.7124	-171.8776
VC2	x	-53.848	-74.744	89.7407	99.2882	-138.3831	-167.4825
	y	-63.9668	-84.3814	80.4094	90.5124	-138.3831	-167.4825

	z	-323.1	-376.4	-170.15	-189.801	-138.3831	-167.4825
VC3	x	-64.2985	-86.084	88.0167	96.92	-146.4809	-175.8674
	y	-66.5068	-87.5992	85.7613	95.3199	-146.4809	-175.8674
	z	-337	-389.4	-173.778	-192.24	-146.4809	-175.8674
VC4	x	-64.56	-86.707	87.3718	96.784	-146.1104	-176.3553
	y	-66.3688	-88.0397	85.511	95.3683	-146.1104	-176.3553
	z	-335.9	-389.9	-172.883	-192.152	-146.1104	-176.3553

Examining Table 1, the FC term is isotropic for all VCs while the SD term is anisotropic. The FC term is about 50% larger than the SD term. B3LYP gives us larger values for both SD and FC. The HC values for the four VCs do not vary much, which is consistent with the localized nature of electron spins. This vanadyl motif gives us consistent vanadium HC regardless of the lengths of the ligands attached.

Table 2. A comparison of the experimental & theoretical HC values for VC1. Two functionals BP & B3LYP were compared for elements V and H.

Element	$\|A\|$ (MHz)		
	Experiment	Theory	
		B3LYP	BP
V	379	392	348
H	N/A	14.1	14.3

From Table 2, we can see that the HC values for V are much greater than those for H for VC1. Since the value for H decays as the lengths of the ligands grow, the vanadium HC is always the dominant contribution to total HC in these series of VCs. Based on that, it is expected

to have the biggest effect on the coherence time T_2. The vanadium HC value using B3LYP is within 10% of the experimental HC value.

Fig. 6 and 7 are graphs of how the average hydrogen HC changes with distance. The nuclear spin is on the central vanadium atom and an electron spin is on each of the seven hydrogens that contribute to decoherence. For the power (logarithmic) fit, the trend is $\frac{1}{r^3}$, which matches the SD Hamiltonian:

$$H_{SD} = \frac{\mu_0 g_p e^2}{8\pi m_p m_e} \frac{\left[3(\mathbf{S_p}\cdot\hat{r})(\mathbf{S_e}\cdot\hat{r}) - \mathbf{S_p}\cdot\mathbf{S_e}\right]}{r^3} \tag{45}$$

where μ_0 is the permeability of the vacuum, g_p is the g-factor for the proton, e is the charge of the electron and m_p & m_e are the masses for the proton and electron respectively. The power fit for all the VCs is $y = \frac{181.5}{x^{2.88}}$. If VC1 is excluded, the fit becomes closer to the expected trend: $y = \frac{215.9}{x^{3.027}}$. This makes sense because the SD term should dominate at longer distances.

Looking at the root-means squared (RMS) values of the fits, the power fit is much better than exponential. With the VC1 data points, the RMS is .1050 MHz for the power fit and 12.661 MHz for the exponential fit. Without the VC1 data points, the RMS value decreases to .0076 MHz for the power fit and 4.1973 MHz for the exponential fit.

Shown by the decrease in RMS values in Fig. 6 and 7 when the VC1 data points are removed, significant deviation from the fitted curves only happens for VC1. This deviation comes from the FC term, which does not contribute significantly for molecules with wider branches. Since the FC term arises from the overlap of the nuclear and electron wavefunction, it makes sense that at longer distances the FC is negligible. The HC can be modeled through SD interactions alone for large molecules. This can be confirmed by looking at the ratio between FC and SD vs. distance in Fig. 8 below.

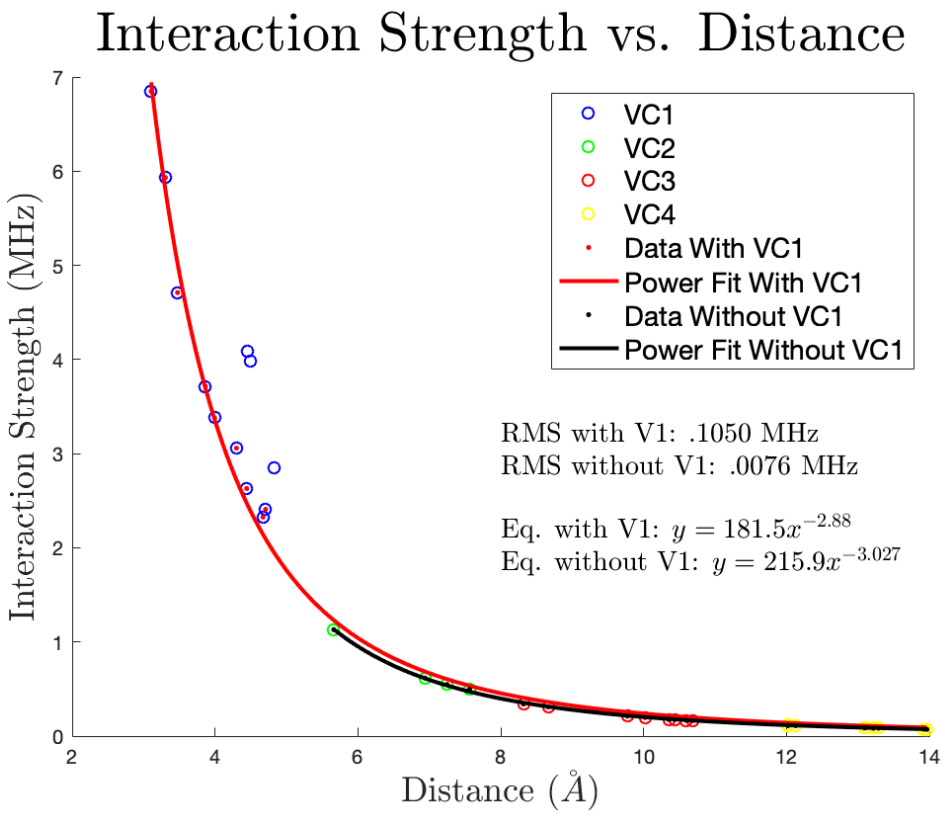

Fig. 6 Graph of HC vs. distance with two power fits respectively including and not including VC1. Three outlier data points in VC1 were not included in the fits.

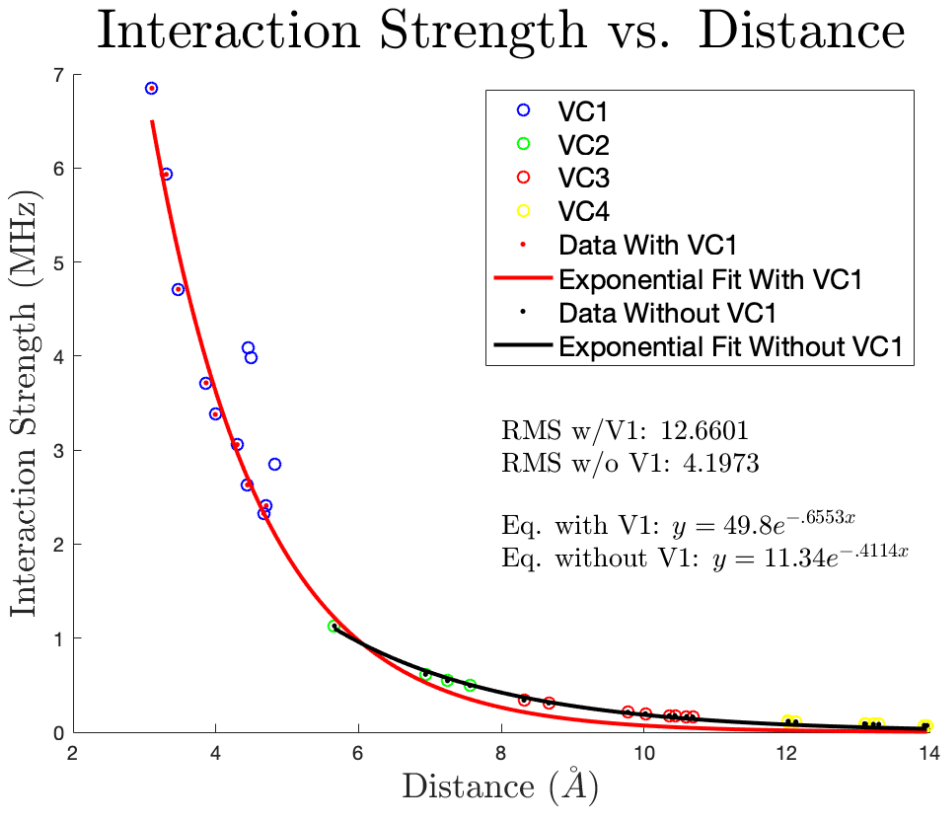

Fig. 7 Graph of HC vs. distance with two exponential fits respectively including and not including VC1. Three outlier data points in VC1 were not included in the fits.

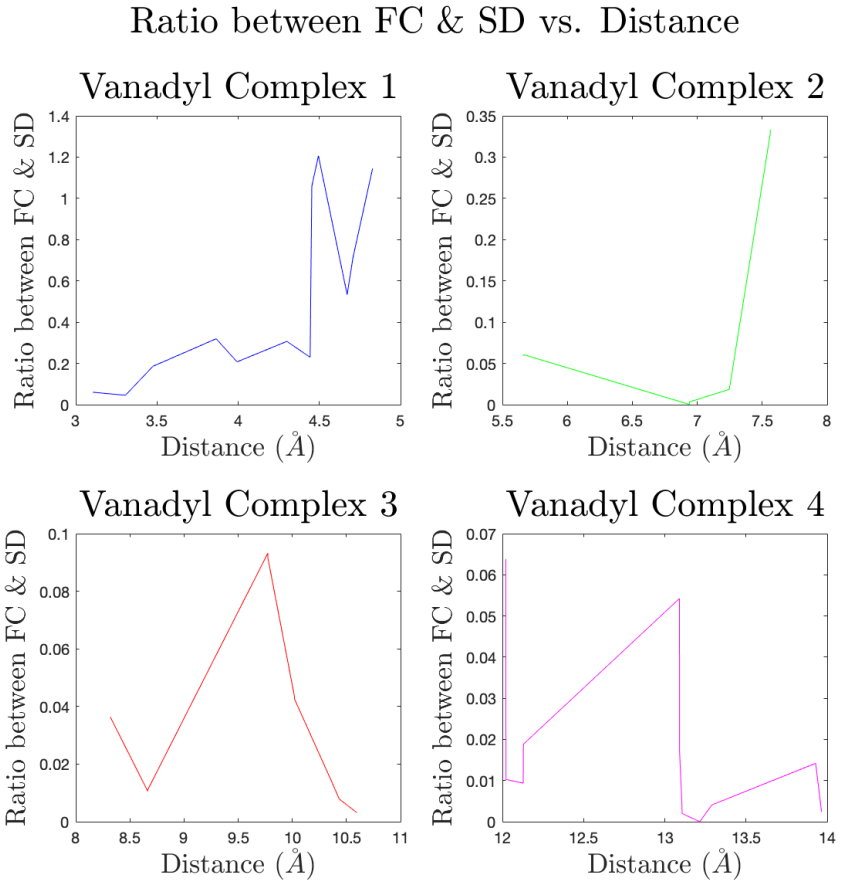

Fig. 8 Graph of the ratio of FC/SD vs. distance of the average bond length.

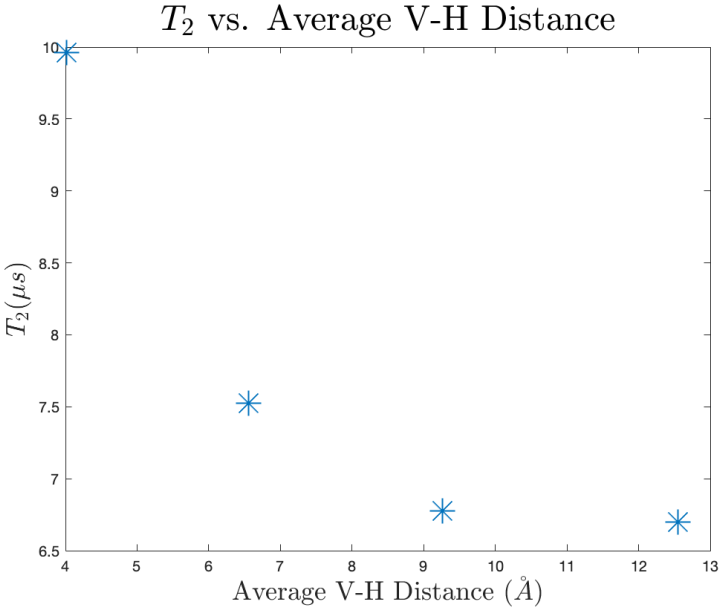

Fig. 9 Graph of the experimental values of T_2 vs. Average V-H Distance from Dr. Freedman's study [9].

Using Eq. 30, T_2 was calculated to be around .03 μs for four VCs. Comparing to experimental values it is off by around a factor of 10^2. Eq. 30 gave the same T_2 for all the VCs, when it should vary like the graph above. HC coupling stays the same, but T_2 becomes smaller as the length of the ligands becomes longer, so this theory does not explain the trend observed in experiments. One possible explanation for this interesting phenomenon is the diffusion barrier.

When the V-H distance is less than the diffusion barrier radius, the nuclear and electron spins are so strongly coupled the electron flips do not happen on an experimental time-scale and do not contribute to decoherence. Vanadium and hydrogen HC in VC1 do not contribute to T_2 significantly. One possible reason this stochastic theory does not match experiment is that it does not account for the diffusion barrier.

Conclusion

DFT calculations determined that the orbitals are localized on the vanadium ion, but the electron spins are neither HOMO nor LUMO in these molecules. The HC values for V are much greater than those for H. Using B3LYP, we can obtain reasonable HC values for V when compared to experiment. For H, significant deviation of HC only happens for VC1. This deviation comes from the FC term, which is negligible for molecules with wider branches. The HC can be modeled using only spin-dipole interactions for large molecules. Estimations based on the Kubo-Anderson Model are neither able to match experimental T_2 nor explain the observed T_2 trend for this VC family. One possible deviation for this inconsistency that exists in literature is the nuclear diffusion model. The next step for this work is to understand and apply this model to potential candidates of molecular qubits.

Acknowledgments

This research was performed with funds from the NSF for the REU Site: Condensed Matter Physics and Applied Materials (DMR-1852138).

Bibliography

[1] Leuenberger, M.N. and Loss, D., 2001. Quantum computing in molecular magnets. *Nature*, *410*(6830), p.789.

[2] Gaita-Ariño, A., Luis, F., Hill, S. and Coronado, E., 2019. Molecular spins for quantum computation. *Nature chemistry*, *11*(4), p.301.

[3] CB Insights Research (2019).

[4] Kane, B.E., 1998. A silicon-based nuclear spin quantum computer. *nature*, *393*(6681), p.133

[5] Berman, G.P., Doolen, G.D., Hammel, P.C. and Tsifrinovich, V.I., 2000. Solid-state nuclear spin quantum computer based on magnetic resonance force microscopy. *Physical Review B*, *61*(21), p.14694.

[6] R. Hanson, L.P. Kouwenhoven, J.R. Petta, S. Tarucha, and L.M.K. Vandersypen, Reviews of Modern Physics **79**, 1217 (2007).

[7] R. Kubo, "A stochastic theory of line shape," in Advances in Chemical Physics (John Wiley and Sons, Ltd, 1969) pp. 101–127.

[8] P. W. Anderson, Journal of the Physical Society of Japan 9, 316 (1954). Graham, M.J., Yu.

[9] C.J., Krzyaniak, M.D., Wasielewski, M.R. and Freedman, D.E., 2017. Synthetic Approach To Determine the Effect of Nuclear Spin Distance on Electronic Spin Decoherence. *Journal of the American Chemical Society*, *139*(8), pp.3196-3201.

[10] Neese, F., 2002. Prediction and interpretation of the 57Fe isomer shift in Mössbauer spectra by density functional theory. *Inorganica Chimica Acta*, *337*, pp.181-192.

[11] Neese, F., 2012. The ORCA program system. *Wiley Interdisciplinary Reviews: Computational Molecular Science*, *2*(1), pp.73-78.

[12] F. Bloch, Phys. Rev. 70, 460 (1946).

[13] N. Bloembergen, E.M. Purcell, and R. V. Pound, Phys. Rev. 73, 679 (1948).